

Stealthy bias injection attack detection based on Kullback–Leibler divergence in stochastic linear systems

Jingwei Dong, André M. H. Teixeira

ABSTRACT. This paper studies the design of detection observers against stealthy bias injection attacks in stochastic linear systems under Gaussian noise, considering adversaries that exploit noise and inject crafted bias signals into a subset of sensors in a slow and coordinated manner, thereby achieving malicious objectives while remaining stealthy. To address such attacks, we formulate the observer design as a max–min optimization problem to enhance the detectability of worst-case BIAs, which attain a prescribed attack impact with the least detectability evaluated via Kullback–Leibler divergence. To reduce the computational complexity of the derived non-convex design problem, we consider the detectability of worst-case BIAs at three specific time instants: attack onset, one step after attack occurrence, and the steady state. We prove that the Kalman filter is optimal for maximizing the BIA detectability at the attack onset, regardless of the subset of attacked sensors. For the one-step and steady-state cases, the observer design problems are approximated by bi-convex optimization problems, which can be efficiently solved using alternating optimization and alternating direction method of multipliers. Moreover, more tractable linear matrix inequality relaxations are developed. Finally, the effectiveness of the proposed stealth-aware detection framework is demonstrated through an application to a thermal system.

1. INTRODUCTION

To enable high-performance operation in modern industrial infrastructures, including smart grids, intelligent transportation, and manufacturing, cyber-physical systems (CPSs) have been developed by seamlessly integrating communication, computation, control, and physical processes. However, the reliance of CPSs on sensors, communication networks, and IT infrastructures, e.g., Supervisory Control and Data Acquisition systems, exposes them to cyber threats. Adversaries can exploit vulnerabilities in these components to compromise system performance [1, 2]. Conventional information-theoretic security mechanisms, such as encryption, firewalls, and digital watermarking, provide essential protection but ignore the physical dynamics of the controlled plant. Therefore, they may be insufficient against cyber attacks designed from a control-theoretic viewpoint [3]. For instance, such protection schemes failed to prevent the cyber attack on the Davis-Besse nuclear power plant in Ohio, USA [4]. Consequently, there has been growing attention over the past decade to research on the cybersecurity of CPSs from the control-theoretic perspective.

Date: January 22, 2026.

Jingwei Dong and André M. H. Teixeira are with the Department of Information Technology, Uppsala University, SE-75105 Uppsala, Sweden. This work is supported by the Swedish Research Council under the grants 2021-06316 and 2023-05234, the Swedish Foundation for Strategic Research, and the Knut and Alice Wallenberg Foundation.

Cybersecurity research in CPSs can be approached from both the adversarial and defensive perspectives. Specifically, adversaries aim to impair system operation, such as by corrupting state estimation [5] or degrading control performance [6], while remaining undetected. Common attack strategies include denial of service (DoS) attacks, replay attacks, and false data injection (FDI) attacks. According to [7], these attacks can be characterized by three dimensions: model knowledge, disclosure resource, and disruption ability. For example, DoS attacks can degrade system performance by blocking communication channels and require neither system knowledge nor data disclosure, whereas FDI attacks typically rely on model information to generate stealthy attack signals. Another widely used classification groups attacks into deception attacks and DoS attacks. Deception attacks involve tampering with or forging sensing data or control commands to mislead the system; both replay and FDI attacks fall under this category. Extensive studies have explored various attack design methodologies [5–9].

To secure CPSs against cyber attacks, research from the defensive perspective focuses on attack detection and identification [10, 11], resilient state estimation [12], resilient controller design [13], etc. In this work, we investigate the detection of bias injection attacks (BIAs), a particular type of FDI attacks in which adversaries compromise a subset of sensors and slowly inject bias signals to mislead controllers or state estimators. Although BIAs appear simple in form, they can gradually drive system states into unsafe regions and have been extensively studied in the context of power systems [14, 15]. In [16], GPS spoofing was modeled as a zero-sum attacker–defender game, where BIAs emerged as the optimal attack strategy. Moreover, BIAs can be strategically crafted by exploiting system dynamics and noise, and injected into sensors in a coordinated manner to achieve malicious objectives while remaining stealthy [7]. This renders the detection of BIAs under noisy conditions particularly challenging.

1.1. Related work

Attack detection methods in CPSs can be broadly classified into active and passive approaches, each tailored to specific attack types. Specifically, active detection methods, such as moving target defense and watermarking, aim to proactively perturb system dynamics or inputs to expose malicious behaviors, and have been shown to be effective against replay attacks [17, 18]. Passive attack detection methods, mostly derived from residual generation-based fault diagnosis frameworks, are commonly used to detect FDI attacks (including BIAs). For instance, [19] and [20] proposed Kalman filter-based FDI attack detection schemes that integrate statistical detectors using the χ^2 test and the cumulative sum (CUSUM) test, respectively. Observer-based methods have also been employed to estimate attack signals for detection purposes. In [21], the authors developed an unknown input observer to estimate FDI attacks in vehicle platooning systems, while [22] designed an observer based on an augmented system to reconstruct BIA signals. Under the assumption of bounded measurement noise, zonotopic set-membership methods have been adopted to detect bias attacks by checking the consistency between predicted and measured state sets [23, 24]. However, the aforementioned methods generally treat FDI attacks as ordinary anomalies and do not explicitly account for stealthiness (or detectability) and the impact of attacks. As a result, while they may be effective in detecting conventional faults or abrupt anomalies, they can fail to detect bias-type attacks that are deliberately crafted to remain stealthy in the presence of noise.

This challenge highlights the importance of quantifying attack stealthiness in BIA detection strategy design. Regarding the characterization of stealthiness, Pasqualetti et al. [25] showed, from a system-theoretic perspective, that an adversary can construct undetectable attacks by exciting only the zero dynamics of systems with invariant zeros. This result provides a fundamental notion of stealthiness in noiseless systems. In stochastic systems, stealthiness can be reflected in changes in measurement statistics under the effects of both noise and attacks. Early work analyzed attack stealthiness relative to specific detectors, such as bad-data detection [26] and the χ^2 test [27]. To obtain a detector-independent notion of stealthiness, the Kullback–Leibler divergence (KLD) was introduced in [28] as a general measure of statistical distinguishability between attacked and attack-free systems, and has since been widely used in the analysis and design of stealthy FDI attacks in stochastic CPSs [5, 6].

Note that attack stealthiness has been more extensively considered in the context of attack strategy design rather than detection. To our knowledge, existing approaches that explicitly incorporate attack stealthiness into detection strategy design mainly arise in the context of power systems, where structured attacks that directly manipulate state variables to bypass bad data detection mechanisms are considered. The corresponding detection methods are typically based on statistical analysis [29, 30]. However, the static modeling assumptions underlying these approaches limit their applicability to general stochastic dynamical systems. On the other hand, some studies focus on detecting stealthy FDI attacks that lie in undetectable subspaces induced by system structure, such as zero-dynamics attacks [31]. Detecting this type of attacks requires active methods mentioned above, such as modifying system dynamics to break the structural conditions that enable stealthiness.

In contrast, relatively few studies have directly incorporated stealthiness of FDI attacks into residual generation-based detector design for stochastic systems, in which adversaries can deliberately exploit measurement noise to remain stealthy. Since the KLD provides a detector-independent measure of stealthiness for stochastic systems, our previous work [32] employed it to characterize worst-case attack detectability and designed detection observers against the stealthy BIAs. More recently, [33] embedded stealthiness constraints into attack detector design using Wasserstein ambiguity sets, offering another promising research direction. These efforts demonstrate the potential of stealth-aware detection frameworks.

1.2. Main contributions

Building on the above analysis, this paper investigates the detection of BIAs targeting a subset of sensors in linear time-invariant (LTI) systems driven by Gaussian noise. We propose an observer-based detection framework in which both attack stealthiness, quantified using KLD, and attack impact, characterized by a weighted norm of the attack vector, are explicitly incorporated into detector design. The weighting matrix can be selected to reflect specific attack objectives. The contributions of this paper are summarized as follows:

- **Worst-case BIA detector design:** We formulate the observer-based BIA detector design as a max–min optimization problem (as given in (10)) that maximizes the detectability of the worst-case BIAs, which are defined as attack vectors that attain the lowest detectability while ensuring a prescribed impact on the system by comprising only a subset of sensors.

- **Multi-test-instant KLD-based detectability:** To obtain tractable synthesis problems, we consider KLD-based detectability measures at several detection instants, including attack onset, one step after attack occurrence, and the steady-state scenario, providing guarantees on transient and long-term detection performance, respectively. Notably, for the attack-onset case, we show that the Kalman filter is the optimal solution, regardless of the set of compromised sensors and the weighting matrix characterizing attack impact (Proposition 3.4).
- **Observer design via bi-convex approximation:** For the one-step and steady-state cases, the resulting observer design problems are inherently non-convex and computationally intractable. We therefore reformulate them as bi-convex optimization problems in Theorem 3.5 and Theorem 3.8, respectively. Two numerical solution approaches, namely alternating optimization (AO) and the alternating direction method of multipliers (ADMM), are provided to solve the resulting problems.
- **Tractable observer design via linear matrix inequality (LMI) approximation:** The resulting observer design problems for one-step and steady-state cases are further approximated by LMI conditions, as presented in Theorem 3.6 and Theorem 3.9. This leads to computationally tractable observer synthesis procedures at the cost of increased conservatism.

This work constitutes an extension of our previous research [32]. The main differences are summarized as follows: (1) In [32], all sensors are assumed to be potentially compromised, whereas this paper introduces a structured matrix to characterize partially corrupted scenarios, which better reflects the practical situation as some secured sensors are harder to access; (2) The attack impact in [32] was characterized using a positive definite weighting matrix. In contrast, this paper relaxes this assumption and allows the weighting matrix to be positive semidefinite, rendering the methods in [32] inapplicable under this more general setting; (3) The previous work focuses on detector design at the attack onset and the steady-state regime. This paper further considers detector design one step after the attack occurs, thereby enhancing transient detection performance against stealthy BIAs.

The rest of the paper is organized as follows. The problem formulation is introduced in Section 2. Section 3 presents the design methods for the BIA detectors. Section 4 provides the algorithms and the residual evaluation approach. The proposed approaches are applied to a thermal system in Section 5 to illustrate their effectiveness. Section 6 concludes the paper with future directions. To improve the flow of the paper and its accessibility, some technical proofs are relegated to Appendix A.

Notation. Sets \mathbb{N} , \mathbb{R} (\mathbb{R}_+), and \mathbb{R}^n denote non-negative integers, (positive) reals, and the space of n dimensional real vectors, respectively. The identity matrix with an appropriate dimension is denoted by I . For a matrix A , $\rho(A)$ denotes its spectral radius, i.e., the largest amplitude of all eigenvalues of A , and A^\top denotes the transpose of A . We use $A \succ 0$ ($\succeq 0$) to denote a positive (semi-)definite matrix. The set of symmetric positive (semi-)definite matrices is denoted by $\mathbb{S}_{\succ 0}^n$ ($\mathbb{S}_{\succeq 0}^n$). The symbol $*$ is used to denote the off-diagonal elements in symmetric matrices to avoid clutter. For a matrix pair (A, B) , its generalized eigenvalues σ_i satisfy the equality $A\nu = \sigma_i B\nu$ for non-zero vector ν . The smallest generalized eigenvalue is denoted by $\sigma_{\min}(A, B) = \min_{\nu \neq 0, \nu^\top B\nu > 0} \frac{\nu^\top A\nu}{\nu^\top B\nu}$. The quadratic norm of vector v with respect to $W \succeq 0$ is defined as $\|v\|_W^2 = v^\top W v$.

2. MODEL DESCRIPTION AND PROBLEM STATEMENT

This section first presents the system model considered in this work. The formulation of BIAs is then introduced, followed by their impact analysis, stealthiness characterization, and derivation of worst-case BIAs. Finally, the observer design problem against BIAs is formulated.

2.1. System model

Consider the following discrete-time LTI system

$$\begin{cases} x(k+1) = Ax(k) + Bu(k) + B_\omega\omega(k) \\ y(k) = Cx(k) + D_\omega\omega(k) + y_a(k), \end{cases} \quad (1)$$

where $x(k) \in \mathbb{R}^{n_x}$, $u(k) \in \mathbb{R}^{n_u}$, and $y(k) \in \mathbb{R}^{n_y}$ are the state, control input, and measurement output, respectively. The noise term $\omega(k) \in \mathbb{R}^{n_\omega}$ is assumed to be independent identically distributed (i.i.d) Gaussian white noise with zero mean, i.e., $\omega(k) \sim \mathcal{N}(0, I_{n_\omega})$. The signal y_a denotes the sensor attack. The matrices A , B , and C are known system matrices with appropriate dimensions, determined by the plant dynamics and structure. The matrices B_ω and D_ω characterize the effect of noise on the system.

Assumption 2.1. *The pair (A, C) is detectable and the pair (A, B_ω) is stabilizable.*

We employ an observer to monitor the status of the system

$$\begin{cases} \hat{x}(k+1) = A\hat{x}(k) + Bu(k) + L(y(k) - \hat{y}(k)) \\ \hat{y}(k) = C\hat{x}(k), \end{cases} \quad (2)$$

where $\hat{x}(k) \in \mathbb{R}^{n_x}$ and $\hat{y}(k) \in \mathbb{R}^{n_y}$ are estimates of the state and output, respectively. The observer gain $L \in \mathbb{R}^{n_x \times n_y}$ is the parameter to be determined. Define the state estimation error as $\tilde{x}(k) = x(k) - \hat{x}(k)$, whose dynamics are given by

$$\begin{cases} \tilde{x}(k+1) = (A - LC)\tilde{x}(k) + (B_\omega - LD_\omega)\omega(k) - Ly_a(k) \\ r(k) = C\tilde{x}(k) + D_\omega\omega(k) + y_a(k), \end{cases} \quad (3)$$

where $r(k) = y(k) - \hat{y}(k)$ is the residual used to indicate the occurrences of anomalies in the system. Ideally, in the absence of attacks, $r(k)$ fluctuates around zero because of noise, whereas it deviates significantly from zero when attacks or other anomalies occur.

2.2. BIA characterization

In this subsection, we provide a detailed description of the attack signal y_a . Consider the BIA model characterized by a step signal as follows

$$y_a(k) = D_a a(k) = \begin{cases} 0, & k < k_0, \\ D_a \bar{a}, & k \geq k_0, \end{cases} \quad (4)$$

where $\bar{a} \in \mathbb{R}^{n_a}$ is a constant attack vector, and n_a represents the number of compromised sensors. The matrix $D_a \in \mathbb{R}^{n_y \times n_a}$ characterizes the set of unsecured sensors. In particular, let $j_1 < j_2 < \dots < j_{n_a}$ be the indices of sensors that are potentially compromised by the attacker. Then, the elements $(j_1, 1), (j_2, 2), \dots, (j_{n_a}, n_a)$ of D_a are set to one, while all other entries are zero. We further assume that attacks happen at the time instant $k_0 = 0$ and that the error dynamics (3) have reached

steady state by then. This assumption is for notational convenience. According to Assumption 2.1, there always exists an L to stabilize (3), such that the initial estimation error decays exponentially to zero.

2.2.1. Impact of BIAs. BIAs operate by injecting the constant bias \bar{a} into the system to degrade system performance while remaining as stealthy as possible. To quantify such an impact, we introduce the following weighted norm

$$\|D_a \bar{a}\|_W^2 = \bar{a}^\top D_a^\top W D_a \bar{a}, \quad (5)$$

where $W \succeq 0$ is a symmetric positive semidefinite matrix. It is worth noting that (5) provides a general framework to characterize the BIA impact. Specifically, the choice of the weighting matrix W can be adjusted to different objectives, such as increasing the mean square estimation error of system states [34], deviating the steady state from the equilibrium point [7], or degrading the control performance of a linear quadratic Gaussian regulator [35].

To further clarify the selection of the weighting matrix W , we illustrate its construction through a brief example. Consider an output feedback controller $u = Ky$ in (1). In the worst-case scenario, the attacker possesses perfect knowledge of the system and seeks to shift the steady state of the system away from its equilibrium. From the closed-loop dynamics, the steady-state value $x_{a,\infty}$ induced by the attack vector \bar{a} is derived as

$$x_{a,\infty} = (I - (A + BKC))^{-1} B K D_a \bar{a} = G_{y_a x} D_a \bar{a},$$

where $G_{y_a x}$ is the steady-state gain of the transfer function from y_a to x . In this setting, the weighting matrix in (5) is chosen as $W = G_{y_a x}^\top G_{y_a x}$.

2.2.2. Stealthiness characterization of BIA. Given the stochastic nature of the residual induced by noise, we employ the KLD as the measure of attack stealthiness, which captures the discrepancy between the distributions of the attacked and attack-free residuals. The definition of KLD is given as follows.

Definition 2.2 (KLD [36]). *Let p and q be two random vectors with probability density functions $f_p(\cdot)$ and $f_q(\cdot)$, respectively. Then, the KLD between p and q is*

$$\mathcal{D}(p||q) = \int_{\{\zeta: f_p(\zeta) > 0\}} f_p(\zeta) \log \frac{f_p(\zeta)}{f_q(\zeta)} d\zeta.$$

Note that the KLD is non-negative and, in general, non-symmetric. A smaller KLD indicates greater similarity between the two distributions. It equals zero only for identical distributions, i.e., $\mathcal{D}(p||q) = 0 \Leftrightarrow f_p = f_q$.

To compute the KLD between the distributions of the attacked and attack-free residuals, we analyze the statistical characteristics of the residuals in both cases. First, define the attack-free residual signal as r_ω . Based on the error dynamics (3) and the linear stochastic system theory, if $A - LC$ is Schur, the estimation error \tilde{x} in the steady state is subject to $\lim_{k \rightarrow \infty} \tilde{x}(k) \sim \mathcal{N}(0, \Sigma_{\tilde{x}})$. The steady-state covariance matrix $\Sigma_{\tilde{x}}$ is the solution to the following discrete-time Lyapunov equation

$$\Sigma_{\tilde{x}} = (A - LC)\Sigma_{\tilde{x}}(A - LC)^\top + (B_\omega - LD_\omega)(B_\omega - LD_\omega)^\top. \quad (6)$$

Furthermore, the residual r_ω follows $\lim_{k \rightarrow \infty} r_\omega(k) \sim \mathcal{N}(0, \Sigma_{r_\omega})$ with $\Sigma_{r_\omega} = C\Sigma_{\tilde{x}}C^\top + D_\omega D_\omega^\top$.

Second, let r_a denote the residual in the presence of BIAs. By the superposition principle, r_a comprises two components, i.e., $r_a = r_\omega + \bar{r}_a$, where r_ω is the part induced by noise whose distribution has been specified above, and \bar{r}_a is the deterministic contribution from the attack \bar{a} . Recalling that the attack is assumed to start at $k_0 = 0$ with the system initially in the steady state, the attacked component \bar{r}_a is derived as

$$\bar{r}_a(k) = \left(I - C \sum_{l=0}^{k-1} (A - LC)^{k-l-1} L \right) D_a \bar{a} = \Phi(k, L) D_a \bar{a}. \quad (7)$$

For $k = 0$, $\Phi(0, L)$ is defined as the identity matrix I . As a result, the residual under attack at the k -th step follows a Gaussian distribution, i.e., $r_a(k) \sim \mathcal{N}(\bar{r}_a(k), \Sigma_{r_\omega})$. Based on Definition 2.2, the KLD between r_a and r_ω that quantifies the stealthiness of \bar{a} at time k can be computed by

$$\begin{aligned} \mathcal{D}(r_a(k) || r_\omega(k)) &= \frac{1}{2} \bar{r}_a^\top(k) \Sigma_{r_\omega}^{-1}(L) \bar{r}_a(k) \\ &= \frac{1}{2} \bar{a}^\top D_a^\top \Phi^\top(k, L) \Sigma_{r_\omega}^{-1}(L) \Phi(k, L) D_a \bar{a}. \end{aligned} \quad (8)$$

While some studies adopt horizon-based KLD to characterize attack detectability [6], these approaches require long observation horizons and high-dimensional statistical modeling, which limits their suitability for detector synthesis. In contrast, this work adopts the instantaneous KLD in (8) as a measure of attack detectability. Under Gaussian assumptions, it is closely related to the Mahalanobis distance and classical χ^2 tests (outlined in Section 4), thereby providing a natural link to residual-based detection. Moreover, the single-instant consideration enables tractable detection observer design, as developed in the subsequent sections.

2.2.3. Worst-case BIA design. In this subsection, given the BIA impact characterized by the weighted norm in (5) and the stealthiness quantified by the KLD in (8), we present a worst-case BIA design approach that minimizes the KLD between attack-free and attacked residuals while ensuring a prescribed level of attack impact. Accordingly, the worst-case BIA vector denoted by \bar{a}^* is obtained as the solution to the following optimization problem:

$$\begin{aligned} J_k(L) &= \min_{\bar{a} \in \mathbb{R}^{n_a}} \frac{1}{2} \bar{a}^\top D_a^\top \Phi^\top(k, L) \Sigma_{r_\omega}^{-1}(L) \Phi(k, L) D_a \bar{a} \\ \text{s.t. } & \bar{a}^\top D_a^\top W D_a \bar{a} \geq \epsilon, \end{aligned} \quad (9)$$

where $J_k(L)$ represents the smallest KLD value at time k and $\epsilon \in \mathbb{R}_+$ is the lower bound on the BIA impact. Since both the objective and the impact constraint are homogeneous quadratic forms, we may restrict the search to the boundary, and an optimal solution can be chosen to satisfy the equality constraint, i.e., $\bar{a}^\top D_a^\top W D_a \bar{a} = \epsilon$. Without loss of generality, we further set $\epsilon = 1$.

Let us define $\Psi(k, L) = \frac{1}{2} D_a^\top \Phi^\top(k, L) \Sigma_{r_\omega}^{-1}(L) \Phi(k, L) D_a$ and $\Gamma = D_a^\top W D_a$. Note that for a fixed time instant k and a known observer gain L , the worst-case BIA \bar{a}^* to the optimization problem (9) can be obtained by computing the smallest generalized eigenvalue of the matrix pair $(\Psi(k, L), \Gamma)$ [37], as denoted by $\sigma_{\min}(\Psi(k, L), \Gamma)$. In what follows, we outline the derivation of the worst-case BIA in two cases: when Γ is positive definite and when it is positive semidefinite.

(1) **Matrix Γ is positive definite.** The worst-case BIA \bar{a}^* is given by

$$\bar{a}^* = \pm \frac{\sqrt{\epsilon}}{\|v_{\text{pd}}^*\|_\Gamma} v_{\text{pd}}^*,$$

where v_{pd}^* is the eigenvector corresponding to $\sigma_{\min}(\Psi(k, L), \Gamma)$.

(2) **Matrix Γ is positive semidefinite.** When Γ is singular, \bar{a}^* must not lie in the null space of Γ , otherwise, the impact constraint in (9) is not satisfied. Therefore, we first perform eigenvalue decomposition and obtain

$$\Gamma = \begin{bmatrix} U_r & U_n \end{bmatrix} \begin{bmatrix} \Lambda & 0 \\ 0 & 0 \end{bmatrix} \begin{bmatrix} U_r^\top \\ U_n^\top \end{bmatrix},$$

where U_r and U_n contain eigenvectors corresponding to non-zero and zero eigenvalues, respectively. The diagonal matrix Λ contains the non-zero eigenvalues. Note that $\text{rank}(\Gamma) = \text{rank}(U_r) = m < n_a$. Then, by parameterizing $\bar{a} = U_r b$ for $b \in \mathbb{R}^m$, we obtain the reduced optimization problem:

$$J_k(L) = \min_{b \in \mathbb{R}^m} b^\top U_r^\top \Psi(k, L) U_r b, \quad \text{s.t. } b^\top \Lambda b \geq \epsilon.$$

The optimal \bar{a}^* is then obtained by

$$\bar{a}^* = U_r b^* = \pm U_r \frac{\sqrt{\epsilon}}{\|v_{\text{psd}}^*\|_\Lambda} v_{\text{psd}}^*,$$

where v_{psd}^* is the eigenvector corresponding to $\sigma_{\min}(U_r^\top \Psi(k, L) U_r, \Lambda)$.

For further details on the generalized eigenvalue optimization problem and its application to BIA design, we refer readers to [7, 34].

2.3. Problem statement

To enhance the detectability of worst-case BIAs, this study aims to maximize the smallest KLD value $J_k(L)$ in (9) by optimizing the observer gain L . Note that $J_k(L)$ is time-varying, which leads to different objective functions at different time steps k . Nonetheless, we focus on several specific instants because detection performance need not be guaranteed at every time step and $J_k(L)$ contains higher-order terms in L (for $1 < k < \infty$), resulting in increased computational complexity. Specifically, (1) **transient** detection performance can be improved by considering the attack onset at $k = 0$ or one step after attack occurrence at $k = 1$, and (2) **steady-state** detection performance can be enhanced by considering the limit case $k \rightarrow \infty$. Then, we formulate the problem addressed in this paper.

Problem 2.3 (Optimal detection observer design against worst-case BIAs). *Consider the error dynamics (3) and the worst-case BIA in (9). For $k = 0, 1, \infty$, design the observer gain L through the following optimization problem*

$$\max_{L \in \mathbb{R}^{n_x \times n_y}} \{J_k(L) : \rho(A - LC) < 1\}, \quad (10)$$

where $\rho(A - LC) < 1$ is introduced to ensure the stability of the closed-loop estimator.

Remark 2.4 (Non-convexity of the observer design problem). *Although the time instant k has been specified, the resulting optimization problem (10) still remains highly nonlinear and computationally intractable due to the following reasons: (1) The objective function involves the inverse of the residual covariance matrix, i.e., $\Sigma_{r_\omega}^{-1}(L)$, where $\Sigma_{r_\omega}(L)$ itself is a nonlinear function of L according to the discrete-time Lyapunov equation (6); (2) For the cases $k = 1$ and $k \rightarrow \infty$, the composite structure $\Phi^\top(k, L)\Sigma_{r_\omega}^{-1}(L)\Phi(k, L)$ further complicates the objective function; (3) The stability constraint introduces additional nonlinearity into the problem.*

3. MAIN RESULTS

To address the intractability of the original optimization problem (10), we first introduce several lemmas in this section. Leveraging these results, the problem (10) for $k = 1$ and $k = \infty$ is then formulated into more tractable bi-convex and LMI forms. Let us start by reformulating the optimization problem (10) using the Lagrange dual in the following lemma.

Lemma 3.1 (Reformulation of the observer design problem via Lagrange dual). *The optimization problem (10) used for observer design can be reformulated as*

$$\begin{aligned} \max_{L \in \mathbb{R}^{n_x \times n_y}, \lambda \in \mathbb{R}_+} \quad & \lambda \\ \text{s.t.} \quad & \frac{1}{2} D_a^\top \Phi^\top(k, L) \Sigma_{r_\omega}^{-1}(L) \Phi(k, L) D_a - \lambda D_a^\top W D_a \succeq 0, \end{aligned} \quad (11a)$$

$$\rho(A - LC) < 1. \quad (11b)$$

Proof. The Lagrangian of (9) is first obtained as

$$\mathcal{L}(\bar{a}, \lambda) = \frac{1}{2} \bar{a}^\top D_a^\top \Phi^\top(k, L) \Sigma_{r_\omega}^{-1}(L) \Phi(k, L) D_a \bar{a} + \lambda(1 - \bar{a}^\top D_a^\top W D_a \bar{a}),$$

where $\lambda \in \mathbb{R}_+$ is the Lagrange multiplier. The corresponding Lagrange dual function $g(\lambda)$, which is the minimum value of the Lagrangian $\mathcal{L}(\bar{a}, \lambda)$ over \bar{a} , is derived as

$$g(\lambda) = \min_{\bar{a} \in \mathbb{R}^{n_a}} \mathcal{L}(\bar{a}, \lambda) = \begin{cases} \lambda, & \frac{1}{2} D_a^\top \Phi^\top(k, L) \Sigma_{r_\omega}^{-1}(L) \Phi(k, L) D_a \\ & - \lambda D_a^\top W D_a \succeq 0, \\ -\infty, & \text{otherwise.} \end{cases}$$

Given the fact that strong duality holds for any optimization problem with a quadratic objective function and one quadratic inequality constraint [38, Chapter 5.2], the obtained Lagrange dual optimization problem shares an identical optimal value with that of (9), i.e.,

$$\begin{aligned} J_k(L) = \max_{\lambda \in \mathbb{R}_+} \quad & \lambda \\ \text{s.t.} \quad & \frac{1}{2} D_a^\top \Phi^\top(k, L) \Sigma_{r_\omega}^{-1}(L) \Phi(k, L) D_a - \lambda D_a^\top W D_a \succeq 0. \end{aligned}$$

Taking the constraint $\rho(A - LC) < 1$ into account, we reformulate the max-min optimization problem (10) into (11) by jointly optimizing over L and λ . This completes the proof. \square

As discussed in Remark 2.4, the inverse of the covariance matrix $\Sigma_{r_\omega}^{-1}(L)$ in constraint (11a) poses a great challenge in solving the optimization problem. To address this issue, we introduce the following lemma that provides a lower relaxation of $\Sigma_{r_\omega}^{-1}(L)$ while ensuring the stability condition.

Lemma 3.2 (Relaxation of the inverse covariance matrix). *Consider the error dynamics (3) and the inverse of the covariance matrix $\Sigma_{r\omega}^{-1}(L)$. The following statements hold true:*

- (1) $\rho(A - LC) < 1$,
- (2) $\Sigma_{r\omega}^{-1}(L) \succeq (CP^{-1}C^\top + D_\omega D_\omega^\top)^{-1} \succeq \tilde{Z}$,

if there exist symmetric positive definite matrices P and \tilde{Z} such that the following inequalities are satisfied:

$$\begin{bmatrix} P & P(A - LC) & P(B_\omega - LD_\omega) \\ * & P & 0 \\ * & * & I \end{bmatrix} \succ 0, \quad \begin{bmatrix} \tilde{Z} & \tilde{Z}C & \tilde{Z}D_\omega \\ * & P & 0 \\ * & * & I \end{bmatrix} \succ 0. \quad (12)$$

Proof. The first inequality in (12) implies that

$$\begin{bmatrix} P & P(A - LC) \\ * & P \end{bmatrix} \succ 0,$$

which is equivalent to $P - (A - LC)^\top P(A - LC) \succ 0$ according to Schur complement. This ensures the stability of the error dynamics (3), i.e., $\rho(A - LC) < 1$.

For the second statement, we first show that $P^{-1} \succ \Sigma_{\tilde{x}}$ if the first inequality in (12) holds. By utilizing the Schur complement, we have

$$P - \begin{bmatrix} P(A - LC) & P(B_\omega - LD_\omega) \end{bmatrix} \begin{bmatrix} P & 0 \\ * & I \end{bmatrix}^{-1} \begin{bmatrix} (A - LC)^\top P \\ (B_\omega - LD_\omega)^\top P \end{bmatrix} \succ 0.$$

Pre- and post-multiplying the above inequality by P^{-1} and reversing its direction lead to

$$(A - LC)P^{-1}(A - LC)^\top - P^{-1} + (B_\omega - LD_\omega)(B_\omega - LD_\omega)^\top \prec 0.$$

Recall that the covariance matrix $\Sigma_{\tilde{x}}$ is the solution to the discrete-time Lyapunov equation in (6). It holds that $(B_\omega - LD_\omega)(B_\omega - LD_\omega)^\top = \Sigma_{\tilde{x}} - (A - LC)\Sigma_{\tilde{x}}(A - LC)^\top$. By substituting this relation into the above inequality, we have

$$(A - LC)(P^{-1} - \Sigma_{\tilde{x}})(A - LC)^\top - (P^{-1} - \Sigma_{\tilde{x}}) \prec 0.$$

Since $A - LC$ is Schur, according to the discrete-time Lyapunov stability results in [39, Theorem 8.4], $P^{-1} - \Sigma_{\tilde{x}}$ should be a symmetric positive definite matrix, i.e., $P^{-1} \succ \Sigma_{\tilde{x}}$, which further implies that $\Sigma_{r\omega}^{-1}(L) = (C\Sigma_{\tilde{x}}C^\top + D_\omega D_\omega^\top)^{-1} \succeq (CP^{-1}C^\top + D_\omega D_\omega^\top)^{-1}$.

To show $(CP^{-1}C^\top + D_\omega D_\omega^\top)^{-1} \succeq \tilde{Z}$, by pre- and post-multiplying the second inequality in (12) by $\text{diag}(\tilde{Z}^{-1}, I, I)$, the inequality is readily from the Schur complement, which is

$$\tilde{Z}^{-1} - \begin{bmatrix} C & D_\omega \end{bmatrix} \begin{bmatrix} P & 0 \\ * & I \end{bmatrix}^{-1} \begin{bmatrix} C^\top \\ D_\omega^\top \end{bmatrix} = \tilde{Z}^{-1} - (CP^{-1}C^\top + D_\omega D_\omega^\top) \succ 0.$$

This completes the proof. \square

The following lemma characterizes the monotonicity property of the smallest generalized eigenvalues, which is instrumental in establishing the optimality of the Kalman filter at the attack onset.

Lemma 3.3 (Monotonicity of the smallest generalized eigenvalues). *Let X_1 , X_2 , and Y be positive semidefinite matrices with $X_1 \succeq X_2$. The smallest generalized eigenvalues of the pairs (X_1, Y) and (X_2, Y) satisfy*

$$\sigma_{\min}(X_1, Y) \geq \sigma_{\min}(X_2, Y).$$

Proof. For any feasible ν , $X_1 \succeq X_2$ implies that $\nu^\top X_1 \nu \succeq \nu^\top X_2 \nu$, hence $\frac{\nu^\top X_1 \nu}{\nu^\top Y \nu} \geq \frac{\nu^\top X_2 \nu}{\nu^\top Y \nu}$. Recall the expression of the smallest generalized given in notation. Taking the minimum over all feasible ν leads to $\sigma_{\min}(X_1, Y) \geq \sigma_{\min}(X_2, Y)$. If Y is singular, the minimization is taken over vectors ν satisfying $\nu^\top Y \nu > 0$. This completes the proof. \square

We are now ready to present the main results of the paper.

3.1. KLD-based observer design for attack-onset detectability

We first consider the case $k = 0$ in (10), which aims to enhance the detectability of worst-case BIAs at the attack onset. According to (7), the contribution of BIAs to the residual at $k = 0$ is $\bar{r}_a(0) = \Phi(0, L)D_a\bar{a}$, where $\Phi(0, L) = I$ is the identity matrix. Consequently, the reformulated optimization problem (11) for observer design becomes

$$\begin{aligned} J_0(L_0^*) &= \max_{L \in \mathbb{R}^{n_x \times n_y}, \lambda \in \mathbb{R}_+} \lambda \\ \text{s.t. } & \frac{1}{2}D_a^\top \Sigma_{r_\omega}^{-1}(L)D_a - \lambda D_a^\top W D_a \succeq 0 \text{ and (11b),} \end{aligned} \tag{13}$$

where L_0^* is the optimal solution to (13) and $J_0(L_0^*)$ denotes the optimal objective value. The following proposition shows that the Kalman filter is optimal with respect to onset detectability.

Proposition 3.4 (Optimality of the Kalman filter at attack onset). *For the attack-onset case, i.e., $k = 0$, the Kalman filter is the optimal solution to the reformulated optimization problem (13) for the worst-case BIA detection observer design, irrespective of the set of compromised sensors characterized by D_a and the impact matrix W .*

Proof. Define the feasible set of (11b) as $\mathbb{L} := \{L \in \mathbb{R}^{n_x \times n_y} : \rho(A - LC) < 1\}$. According to Lemma 3.1, for any $L \in \mathbb{L}$, the optimization problem (13) is the dual of (9) at $k = 0$ with zero duality gap, where the optimal value of (9) equals $\sigma_{\min}(\frac{1}{2}D_a^\top \Sigma_{r_\omega}^{-1}(L)D_a, D_a^\top W D_a)$. Therefore, (13) can be interpreted as finding $L \in \mathbb{L}$ that maximizes $\sigma_{\min}(\frac{1}{2}D_a^\top \Sigma_{r_\omega}^{-1}(L)D_a, D_a^\top W D_a)$. According to Lemma 3.3, this is equivalent to finding L that maximizes $\frac{1}{2}D_a^\top \Sigma_{r_\omega}^{-1}(L)D_a$. Since the Kalman filter gain, which is denoted as L_{kal} , minimizes the residual covariance matrix $\Sigma_{r_\omega}(L)$, it holds that $\frac{1}{2}D_a^\top \Sigma_{r_\omega}^{-1}(L_{kal})D_a \succeq \frac{1}{2}D_a^\top \Sigma_{r_\omega}^{-1}(L)D_a$ for all $L \in \mathbb{L}$. As a result, the Kalman filter is the optimal solution to (13) regardless of D_a and W . This completes the proof. \square

3.2. KLD-based observer design for one-step detectability

Setting $k = 1$ in the observer design problem (10) can enhance the detectability of worst-case BIAs one step after their occurrence. According to (7), the contribution of BIAs to the residual

at $k = 1$ becomes $\bar{r}_a(1) = (I - CL)D_a\bar{a}$, where $\Phi(1, L) = I - CL$. Building on Lemma 3.1, the observer design problem for the one-step case becomes

$$\begin{aligned} J_1(L_1^*) &= \max_{L \in \mathbb{R}^{n_x \times n_y}, \lambda \in \mathbb{R}_+} \lambda \\ \text{s.t. } & \frac{1}{2}D_a^\top(I - CL)^\top\Sigma_{r_\omega}^{-1}(L)(I - CL)D_a - \lambda D_a^\top WD_a \succeq 0 \text{ and (11b),} \end{aligned} \quad (14)$$

where L_1^* is the optimal solution to (14) and $J_1(L_1^*)$ is the corresponding optimal objective value. The matrix inequality constraint in (14) is complicated due to the presence of the composite term $D_a^\top(I - CL)^\top\Sigma_{r_\omega}^{-1}(L)(I - CL)D_a$. To address this issue, the following theorem provides a bi-convex approximation of (14) producing a feasible, but possibly suboptimal, solution.

Theorem 3.5 (Bi-convex approximation for one-step detectability). *Consider the error dynamics (3) in the presence of BIAs. The reformulated optimization problem (14) of the detection observer design problem (10) at $k = 1$ can be approximated through the following bi-convex optimization problem*

$$\begin{aligned} \max \quad & \lambda \\ \text{s.t. } & L \in \mathbb{R}^{n_x \times n_y}, \lambda \in \mathbb{R}_+, P \in \mathbb{S}_{\succ 0}^{n_x}, \tilde{Z} \in \mathbb{S}_{\succ 0}^{n_y}, Y \in \mathbb{R}^{n_y \times n_a}, \text{ (12),} \\ & \begin{bmatrix} \varphi(Y, L) - \lambda D_a^\top WD_a & Y^\top \\ Y & \frac{1}{2}\tilde{Z} \end{bmatrix} \succeq 0, \end{aligned} \quad (15)$$

where $\varphi(Y, L) = Y^\top(I - CL)D_a + D_a^\top(I - CL)^\top Y$. The optimal objective value λ^* satisfies $\lambda^* < J_1(L_1^*)$.

Proof. Since $\frac{1}{2}((I - CL)D_a - 2\Sigma_{r_\omega}(L)Y)^\top\Sigma_{r_\omega}^{-1}(L)((I - CL)D_a - 2\Sigma_{r_\omega}(L)Y) \succeq 0$, it holds that

$$\frac{1}{2}D_a^\top(I - CL)^\top\Sigma_{r_\omega}^{-1}(L)(I - CL)D_a \succeq \varphi(Y, L) - 2Y^\top\Sigma_{r_\omega}(L)Y. \quad (16)$$

According to Lemma 3.2, inequalities (12) ensure that $\rho(A - LC) < 1$ and $\Sigma_{r_\omega}^{-1}(L) \succ \tilde{Z}$. Together with inequality (16), we have

$$\frac{1}{2}D_a^\top(I - CL)^\top\Sigma_{r_\omega}^{-1}(L)(I - CL)D_a \succeq \varphi(Y, L) - 2Y^\top\tilde{Z}^{-1}Y. \quad (17)$$

Then, applying the Schur complement to (15) leads to

$$\varphi(Y, L) - 2Y^\top\tilde{Z}^{-1}Y \succeq \lambda D_a^\top WD_a.$$

By substituting (17) into the above inequality, we have

$$\frac{1}{2}D_a^\top(I - CL)^\top\Sigma_{r_\omega}^{-1}(L)(I - CL)D_a - \lambda D_a^\top WD_a \succeq 0.$$

This establishes the sufficiency of the derived conditions in (15), and thus the optimal objective value λ^* provides a lower bound on that of (14). This completes the proof. \square

The optimization problem (15) contains bi-linear terms PL and $Y^\top CL$ in its constraints, which are nonlinear but can be solved efficiently using well-established AO and ADMM algorithms. The implementation of the two algorithms for solving (15) will be outlined in Subsection 4.1. Alternatively, the observer design problem (14) can be further approximated by more tractable LMIs,

albeit at the cost of increased conservatism in the solutions. To this end, the impact matrix W is factorized as $W = R_W^\top R_W$. The result is presented in the following theorem.

Theorem 3.6 (LMI-based approximation for one-step detectability). *Consider the error dynamics (3) in the presence of BIAs. Given a positive scalar $\gamma \in \mathbb{R}_+$, the reformulated optimization problem (14) for detection observer design at $k = 1$, can be approximated through the following LMI-based optimization problem*

$$\begin{aligned} & \min \mu \\ \text{s.t. } & \mu \in \mathbb{R}_+, \quad P \in \mathbb{S}_{\succ 0}^{n_x}, \quad \tilde{Z} \in \mathbb{S}_{\succ 0}^{n_y}, \quad G \in \mathbb{R}^{n_x \times n_y}, \quad Y \in \mathbb{R}^{n_y \times n_a}, \\ & \begin{bmatrix} P & PA - GC & PB_\omega - GD_\omega \\ * & P & 0 \\ * & * & I \end{bmatrix} \succ 0, \quad \begin{bmatrix} \tilde{Z} & \tilde{Z}C & \tilde{Z}D_\omega \\ * & P & 0 \\ * & 0 & I \end{bmatrix} \succ 0, \end{aligned} \quad (18a)$$

$$\begin{bmatrix} \begin{bmatrix} Y^\top D_a + D_a^\top Y & D_a^\top R_W^\top \\ R_W D_a & 2\mu I \end{bmatrix} & \begin{bmatrix} \Gamma_1 & 0 \\ 0 & \mu I \\ \Gamma_2 & 0 \\ 0 & \mu I \end{bmatrix} \\ * & \end{bmatrix} \succeq 0, \quad (18b)$$

and the involved matrices are

$$\Gamma_1 = \begin{bmatrix} Y^\top C & D_a^\top G^\top & Y^\top D_w \end{bmatrix}, \quad \Gamma_2 = \begin{bmatrix} (2 + 1/\gamma)^{-1}P & 0 & 0 \\ * & 1/\gamma P & 0 \\ * & * & 1/2I \end{bmatrix},$$

where $\mu = 1/\lambda$, $W = R_W^\top R_W$ and the observer gain matrix $L = P^{-1}G$.

Proof. The proof is relegated to Section A. □

3.3. KLD-based observer design for steady-state detectability

To enhance the steady-state detectability of worst-case BIAs, we consider $k \rightarrow \infty$ in the optimization problem (11) and obtain:

$$\begin{aligned} J_\infty(L_\infty^*) &= \max_{L \in \mathbb{R}^{n_x \times n_y}, \lambda \in \mathbb{R}_+} \lambda \\ \text{s.t. } & \frac{1}{2} D_a^\top \Phi(\infty, L)^\top \Sigma_{r_\omega}(L)^{-1} \Phi(\infty, L) D_a - \lambda D_a^\top W D_a \succeq 0 \text{ and (11b)}, \end{aligned} \quad (19)$$

where $\Phi(\infty, L) = I - C(I - A + LC)^{-1}L$, L_∞^* is the optimal solution to (19) with $J_\infty(L_\infty^*)$ being the corresponding optimal objective value. To deal with the non-tractable term $\Phi(\infty, L)$ in the constraint, we derive an alternative expression of $\Phi(\infty, L)$ in the following lemma.

Lemma 3.7 (Transformation of the steady-state transition matrix). *Assume that the system matrix A has no unit eigenvalues and $A - LC$ is Schur. The steady-state transition matrix $\Phi(\infty, L)$ in (7) can be written as*

$$\Phi(\infty, L) = (I + ML)^{-1}, \quad (20)$$

where $M = C(I - A)^{-1}$.

Proof. The proof is relegated to Section A. \square

The Schur stability of $(A - LC)$ ensures the existence of a steady-state transition matrix $\Phi(\infty, L)$, while the absence of unit eigenvalues in A guarantees the invertibility of $I - A$. If A has eigenvalues at 1, zero-dynamics attacks \bar{a} can be constructed from the corresponding eigenvectors of A , rendering $\lim_{k \rightarrow \infty} \bar{r}_a = 0$ for any L [7]. Consequently, such attacks remain undetectable in the steady state. Thus, they are excluded from our analysis in this part. For a comprehensive discussion of zero-dynamics attacks and detection strategies, see [31]. With the alternative expression of the steady-state transition matrix in (20), we obtain a bi-convex approximation of the optimization problem (19) in the following theorem.

Theorem 3.8 (Bi-convex approximation for steady-state detectability). *Consider the error dynamics (3) in the presence of BIAs and assume that A has no unit eigenvalues. Utilizing the alternative expression of $\Phi(\infty, L)$ in (20), the reformulated optimization problem (19) for detection observer design at $k = \infty$ can be approximated through the following bi-convex optimization problem*

$$\begin{aligned} & \max \lambda \\ \text{s.t. } & \lambda \in \mathbb{R}_+, L \in \mathbb{R}^{n_x \times n_y}, P \in \mathbb{S}_{>0}^{n_x}, \tilde{Z} \in \mathbb{S}_{>0}^{n_y}, Y \in \mathbb{R}^{n_y \times n_a}, (12), \\ & \begin{bmatrix} D_a^\top Y + Y^\top D_a - \lambda D_a^\top W D_a & Y^\top (I + ML) \\ * & \frac{1}{2} \tilde{Z} \end{bmatrix} \succeq 0. \end{aligned} \quad (21)$$

The optimal objective value λ^* satisfies $\lambda^* < J_\infty(L_\infty^*)$.

Proof. Utilizing the Young's relation in Lemma A.1 leads to

$$\begin{aligned} & \frac{1}{2} D_a^\top (I + ML)^{-\top} \Sigma_{r_\omega}(L)^{-1} (I + ML)^{-1} D_a \\ & \succeq D_a^\top Y + Y^\top D_a - 2Y^\top (I + ML) \Sigma_{r_\omega}(L) (I + ML)^\top Y, \end{aligned} \quad (22)$$

where $(I + ML) \Sigma_{r_\omega}(L) (I + ML)^\top$ is symmetric positive definite as $I + ML$ is invertible. Then, applying Schur complement to (21) and considering the inequality $\Sigma_{r_\omega}(L)^{-1} \succeq \tilde{Z}$ from (12), we have $D_a^\top Y + Y^\top D_a - 2Y^\top (I + ML) \Sigma_{r_\omega}(L) (I + ML)^\top Y - \lambda D_a^\top W D_a \succeq 0$. Together with the inequality (22), it holds that

$$\frac{1}{2} D_a^\top (I + ML)^{-\top} \Sigma_{r_\omega}(L)^{-1} (I + ML)^{-1} D_a - \lambda D_a^\top W D_a \succeq 0.$$

Therefore, constraints in (19) are satisfied. This completes the proof. \square

We would like to highlight that although our previous work [32] also formulates the observer design for steady-state detectability as a bi-convex optimization problem, its derivation relies on the invertibility of W . Thus, the method in [32] is inapplicable under the more general case when W is positive semidefinite. The derived bi-convex optimization problem (21) can be efficiently solved using AO and ADMM as mentioned above. In addition, an LMI-based optimization problem serving as an approximation of (19) is further provided in the following theorem.

Theorem 3.9 (LMI-based approximation for steady-state detectability). *Consider the error dynamics (3) in the presence of BIAs and assume that A has no unit eigenvalues. Given a positive scalar $\gamma \in \mathbb{R}_+$ and the alternative expression of $\Phi(\infty, L)$ in (20), the reformulated optimization*

problem (19) for detection observer design at $k = \infty$ can be approximated through the following LMI-based optimization problem

$$\begin{aligned} & \max \lambda \\ \text{s.t. } & \lambda \in \mathbb{R}_+, \quad P \in \mathbb{S}_{\succ 0}^{n_x}, \quad \tilde{Z} \in \mathbb{S}_{\succ 0}^{n_y}, \quad G \in \mathbb{R}^{n_x \times n_y}, \quad Y \in \mathbb{R}^{n_y \times n_a}, \quad (18a), \\ & \begin{bmatrix} \Theta_1 & \begin{bmatrix} \Theta_2 & \Theta_3 \end{bmatrix} \\ * & \begin{bmatrix} 1/\gamma P & 0 \\ 0 & \gamma P \end{bmatrix} \end{bmatrix} \succeq 0, \end{aligned} \quad (23)$$

where $L = P^{-1}G$ and the involved matrices are defined as

$$\Theta_1 = \begin{bmatrix} D_a^\top Y + Y^\top D_a - \lambda D_a^\top W D_a & Y^\top \\ * & \frac{1}{2}\tilde{Z} \end{bmatrix}, \quad \Theta_2 = \begin{bmatrix} -Y^\top M \\ 0 \end{bmatrix}, \quad \Theta_3 = \begin{bmatrix} 0 \\ G^\top \end{bmatrix}.$$

Proof. The proof is relegated to Section A. \square

Remark 3.10 (Trade-off between transient and steady-state detectability). *Sections 3.2 and 3.3 investigate the detectability of worst-case BIAs in the one-step and steady-state cases, respectively. Building on these results, the two objectives can be jointly considered by formulating a multi-objective optimization problem, which provides a flexible way to balance transient and steady-state detectability. This can be achieved by solving $\max_{L \in \mathbb{R}^{n_x \times n_y}} \{\alpha J_1(L) + (1 - \alpha) J_\infty(L) : \rho(A - LC) < 1\}$, where $\alpha \in [0, 1]$ is the weighting parameter.*

4. ALGORITHMS DESIGN AND RESIDUAL EVALUATION

This section presents the two algorithms, namely, AO and ADMM, to solve the bi-convex optimization problems (15) and (21), followed by the residual evaluation method.

4.1. AO and ADMM algorithms

Let us introduce AO first, which addresses the bi-linear terms (e.g., PL and $Y^\top CL$ in (15), or PL and $Y^\top ML$ in (21)) by partitioning the coupling decision variables into two disjoint sets, e.g., $\{P, Y\}$ and $\{L\}$. At each iteration of AO, one set of variables is fixed while the rest variables are optimized, reducing the problem to a tractable linear optimization problem. This process alternates until convergence or some predefined stopping criteria are met. AO is easy to implement and widely used in practice. When all subproblems are convex, it guarantees convergence to a stationary point. However, it provides no guarantees on convergence rate or global optimality.

When using AO to solve (15) and (21), the algorithm can be initialized with any gain matrix L that ensures $\rho(A - LC)$ is Schur, e.g., the Kalman filter gain. The algorithm terminates either when the solution converges, i.e., $\|L^{(i)} - L^{(i-1)}\|_2 \leq \epsilon$ where $\epsilon \in \mathbb{R}_+$ is the convergence tolerance chosen by users, or when the maximum iteration number N_{ite} is reached. The implementation details of AO in solving (15) and (21) are summarized in Algorithm 1.

In what follows, we present the approach to solving the optimization problems (15) and (21) using ADMM. Let us briefly explain the mechanism of ADMM. By introducing auxiliary variables and constraints, ADMM constructs an augmented Lagrangian and then alternately optimizes the

Algorithm 1 AO for solving BIA detection observer design in (15) and (21).

1. **Initialize:** Consider the optimization problem (15) (or (21)), and choose $L^{(0)}$, ϵ , N_{ite}
2. **Set:** $i = 0$, $L^{(-1)} = 0$
3. **While** $\|L^{(i)} - L^{(i-1)}\|_2 > \epsilon \wedge i < N_{ite}$, **do**
 - (a) **Step 1:** Minimization over $(P, Y, \tilde{Z}, \lambda)$ with $L^{(i)}$

$$(P^{(i+1)}, Y^{(i+1)}) = \arg \min_{P, Y, \tilde{Z}, \lambda} \{-\lambda : (15) \text{ (or (21))}\}$$
 - (b) **Step 2:** Minimization over (L, \tilde{Z}, λ) with $(P^{(i+1)}, Y^{(i+1)})$

$$L^{(i+1)} = \arg \min_{L, \tilde{Z}, \lambda} \{-\lambda : (15) \text{ (or (21))}\}$$
 - (c) $i = i + 1$
 - (g) End while and return $L^{(i)}$

subproblems and Lagrange multipliers to find solutions efficiently. When applying ADMM to (15) and (21), we define auxiliary variables $G = PL$ and $Q = P^{-1}$, yielding $[PQ \ QG] = [I \ L]$. The inequalities (12) in (15) and (21) are replaced with (18a) accordingly. The following augmented Lagrangian can be constructed

$$\mathcal{L}_\eta(\lambda, P, Q, G, L, \Lambda) = -\lambda + \text{tr}(\Lambda^\top ([PQ \ QG] - [I \ L])) + \frac{\eta}{2} \| [PQ \ QG] - [I \ L] \|_2^2,$$

where $\Lambda \in \mathbb{R}^{n_x \times (n_x + n_y)}$ is the Lagrange multiplier associated with the constraint $[PQ \ QG] = [I \ L]$, $\eta \in \mathbb{R}_+$ is the given step size. Then, we can solve the observer gain by minimizing $\mathcal{L}_\eta(\lambda, P, Q, G, L, \Lambda)$ subject to constraints in (15) (or (21)). Note that PQ, QG in $\mathcal{L}_\eta(\lambda, P, Q, G, L, \Lambda)$ and $Y^\top CL$ in (15) (or $Y^\top ML$ in (21)) are bi-linear terms. Thus, these coupling variables can be partitioned into two sets, i.e., $\{P, G, Y\}$ and $\{Q, L\}$, and then updated in an alternative fashion along with the Lagrange multiplier Λ .

Similar to AO, ADMM can be initiated with any L that renders $A - LC$ Schur stable. The initial Q matrix is set as the inverse of the steady-state error covariance matrix induced by the chosen initial L . The algorithm stops when the observer gain matrix converges, i.e., $\|L^{(i)} - L^{(i-1)}\|_2 \leq \epsilon_1$ and $\|[PQ \ QG] - [I \ L]\|_2 \leq \epsilon_2$ or when the maximum number of iterations N_{ite} is reached. We summarize the implementation steps of ADMM in solving (15) and (21) in Algorithm 2.

Remark 4.1 (Initialization with the LMI-based solutions). *The LMI-based approximations (18) and (23) yield convex optimization problems that can be solved efficiently. Despite their conservatism due to the relaxations involved, the LMI-based solutions provide effective initializations for AO and ADMM algorithms.*

4.2. Residual evaluation

The above results provide approaches for designing detection observers such that the generated residuals r are sensitive to worst-case BIAs. However, since these residuals are multi-dimensional and affected by noise, they are not suitable for directly determining the occurrence of attacks. Therefore, we introduce the squared Mahalanobis distance as the residual evaluation function, which is defined as

$$\mathcal{I}(k) = r^\top(k) \Sigma_{r_\omega}^{-1} r(k).$$

Algorithm 2 ADMM for solving BIA detection observer design in (15) and (21).

1. **Initialize:** Consider the optimization problem (15) (or (21)) and the Lagrangian \mathcal{L}_η , and choose $L^{(0)}, Q^{(0)}, \epsilon_1, \epsilon_2, N_{ite}$
2. **Set:** $i = 0, L^{(-1)} = 0, P^{(0)} = (Q^{(0)})^{-1}, G^{(0)} = P^{(0)}L^{(0)}, \Lambda^{(0)} = 0, \eta = 10000$
3. **While** ($\|L^{(i)} - L^{(i-1)}\|_2 > \epsilon_1 \vee \|P^{(i)}Q^{(i)}Q^{(i)}G^{(i)} - [I \ L^{(i)}]\|_2 > \epsilon_2 \wedge i < N_{ite}$, **do**

 - (a) **Step 1:** Minimization over $(P, G, Y, \tilde{Z}, \lambda)$ with $(L^{(i)}, Q^{(i)})$

$$(P^{(i+1)}, G^{(i+1)}, Y^{(i+1)}, \tilde{Z}^{(i+1)}) = \arg \min_{P, G, Y, \tilde{Z}, \lambda} \{\mathcal{L}_\eta : (15) \text{ (or) } (21)\}$$
 - (b) **Step 2:** Minimization over (L, Q, λ) with $(P^{(i+1)}, G^{(i+1)}, Y^{(i+1)}, \tilde{Z}^{(i+1)})$

$$(L^{(i+1)}, Q^{(i+1)}) = \arg \min_{L, Q, \lambda} \{\mathcal{L}_\eta : (15) \text{ (or) } (21)\}$$
 - (c) **Step 3:** Update Λ

$$\Lambda^{(i+1)} = \Lambda^{(i)} + \eta([P^{(i+1)}Q^{i+1}Q^{(i+1)}G^{i+1}] - [I \ L^{(i+1)}])$$
 - (c) $i = i + 1$
 - (g) End while and return $L^{(i)}$

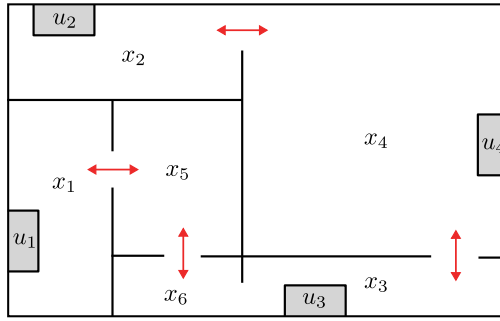


FIGURE 1. Illustration of a six-room thermal system [40].

Note that the Mahalanobis distance characterizes the deviation of a sample from its underlying distribution and is widely used as a measure of statistical discrepancy.

Furthermore, as discussed in Section 2.2.2, residuals in the steady state follow a zero-mean Gaussian distribution in the absence of BIAs. Consequently, the evaluation function $\mathcal{I}(k)$ is subject to a chi-square distribution with n_y degrees of freedom. Its values are concentrated near the origin on the positive real axis with some probability guarantees. In contrast, the presence of attacks changes the residual distribution, leading to a shift in the values of $\mathcal{I}(k)$. Based on this observation, the following detection logic is adopted:

$$\begin{cases} \mathcal{I}(k) \leq \tau, & \text{normal,} \\ \mathcal{I}(k) > \tau, & \text{attack detected.} \end{cases}$$

where the threshold $\tau \in \mathbb{R}_+$ is selected according to a desired false alarm rate ξ , such that the concentration inequality $\mathbb{P}(\mathcal{I}(k) > \tau | a(k) = 0) < \xi$ is satisfied.

5. NUMERICAL EXAMPLES

In this section, the effectiveness of the proposed BIA detection methods is validated through an application to a thermal system.

5.1. Thermal system description

Consider the thermal system depicted in Fig. 1, which consists of six rooms, and four of them are equipped with air-conditioning units. The bidirectional arrows indicate thermal transmission through vents between adjacent rooms, with a thermal transmission rate of 0.1. Each vent is equipped with a sensor that measures the average temperature of the two connected rooms. Let x_i , $i \in \{1, 2, \dots, 6\}$, denote the difference between the temperature in the i th room and the desired set-point. The dynamics of the thermal system can be described by the following state-space model [40]:

$$x(k+1) = \begin{bmatrix} 0.8 & 0 & 0 & 0 & 0.1 & 0 \\ 0 & 0.8 & 0 & 0.1 & 0 & 0 \\ 0 & 0 & 0.7 & 0.1 & 0 & 0.1 \\ 0 & 0.1 & 0.1 & 0.7 & 0 & 0 \\ 0.1 & 0 & 0 & 0 & 0.7 & 0.1 \\ 0 & 0 & 0.1 & 0 & 0.1 & 0.7 \end{bmatrix} x(k) + \begin{bmatrix} I \\ 0_{2 \times 4} \end{bmatrix} u(k),$$

$$y(k) = \begin{bmatrix} 0.5 & 0 & 0 & 0 & 0.5 & 0 \\ 0 & 0.5 & 0 & 0.5 & 0 & 0 \\ 0 & 0 & 0.5 & 0.5 & 0 & 0 \\ 0 & 0 & 0 & 0 & 0.5 & 0.5 \\ 0 & 0 & 0.5 & 0 & 0 & 0.5 \end{bmatrix} x(k).$$

The controller is an output feedback control $u(k) = K\hat{x}(k)$. To characterize the impact of noise, we choose matrices $B_\omega = 0.1[I_6 \ 0_{6 \times 5}]$ and $D_\omega = 0.1[0_{5 \times 6} \ I_5]$.

5.2. Comparison Method

To demonstrate the advantages of the proposed detection observer in detecting stealthy BIAs, we compare it with a recently developed robust residual generator presented in [41], which leverages mixed $\mathcal{H}_2/\mathcal{H}_-$ indices. Specifically, the residual generator guarantees the worst-case anomaly sensitivity by maximizing the \mathcal{H}_- index of the transfer function from anomaly signals to the residual, while simultaneously mitigating noise effects by constraining the \mathcal{H}_2 norm of the transfer function from noise to the residual. To adapt the $\mathcal{H}_2/\mathcal{H}_-$ filter to the BIA detection problem addressed in this paper, and based on the error dynamics in (3), we define the transfer functions from a to r and from ω to r as \mathbb{T}_{ar} and $\mathbb{T}_{\omega r}$, respectively. The gain matrix of the $\mathcal{H}_2/\mathcal{H}_-$ filter can then be obtained by solving the following optimization problem:

$$\max_{L \in \mathbb{R}^{n_x \times n_y}} \left\{ \|\mathbb{T}_{ar}(e^{j\theta})\|_{\mathcal{H}_-([\theta_1, \theta_2])}^2 : \|\mathbb{T}_{\omega r}\|_{\mathcal{H}_2}^2 \leq \delta \right\},$$

where $\|\mathbb{T}_{ar}(e^{j\theta})\|_{\mathcal{H}_-([\theta_1, \theta_2])}$ is the \mathcal{H}_- index of \mathbb{T}_{ar} over the frequency range $[\theta_1, \theta_2]$, with $\theta_1 = \theta_2 = 0$ as the BIA occurs at zero frequency, $\|\mathbb{T}_{\omega r}\|_{\mathcal{H}_2}^2$ is the \mathcal{H}_2 norm of $\mathbb{T}_{\omega r}$, and $\delta \in \mathbb{R}_+$ is an upper bound on $\|\mathbb{T}_{\omega r}\|_{\mathcal{H}_2}^2$. Following the procedure in [41], the optimization problem can be equivalently written as bi-linear matrix inequalities using the Generalized Kalman-Yakubovich-Popov (GKYP) lemma, and can be solved through the AO approach.

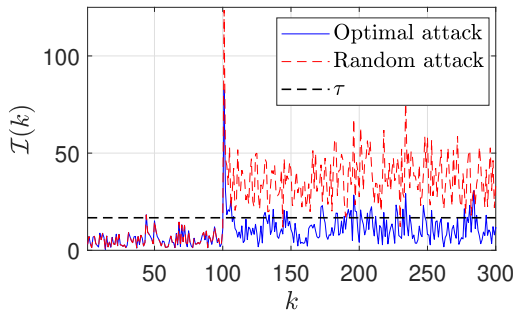


FIGURE 2. Mahalanobis distance using Kalman filter under optimal and random step attacks.

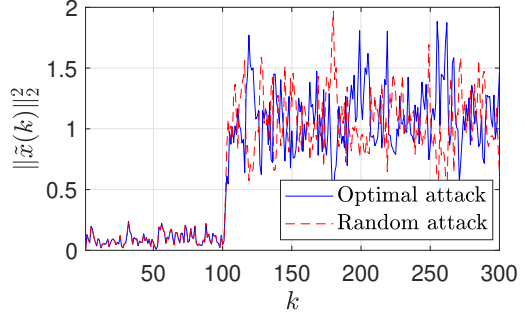


FIGURE 3. Impacts of optimal and random step attacks on state estimation errors.

5.3. Simulation results

We first present the optimal (or worst-case) attack vector \bar{a}_{kal}^* constructed for the Kalman filter. Assume that sensors 1, 3, and 5 in the thermal system are compromised. According to the definition of the attack matrix D_a in Subsection 2.2, the entries (1,1), (3,2), and (5,3) of D_a are equal to 1, and the rest entries are zeros. Suppose that the attack aims to increase the steady-state estimation error of the Kalman filter. According to the error dynamics (3), we have $\lim_{k \rightarrow \infty} \tilde{x}(k) = G_{y_a \tilde{x}} D_a \bar{a}$, where $G_{y_a \tilde{x}} = -(I - (A - L_{kal} C))^{-1} L_{kal}$ is the steady-state transition matrix from y_a to r . Then, following the formulation of the BIA impact in (5), we define the weighting matrix as $W = G_{y_a \tilde{x}}^\top G_{y_a \tilde{x}}$. Given Kalman filter gain L_{kal} and the weighting matrix W , the optimal attack vector \bar{a}^* is the solution to the optimization problem (9) at $k = 0$, which corresponds to the smallest generalized eigenvalue of the matrix pair $(\frac{1}{2} D_a^\top \Sigma_{r_\omega}^{-1} (L_{kal}) D_a, D_a^\top W D_a)$. By calculation, we have $\bar{a}_{kal}^* = [-0.9532 \ 0.0195 \ 0.0425]^\top$.

The stealthiness of the optimal attack is demonstrated in the following simulation results. For comparison, we consider a random attack \tilde{a} , which satisfies the same impact constraint as \bar{a}_{kal}^* , i.e., $\tilde{a}^\top D_a^\top W D_a \tilde{a} = 1$. The random attack used here is $\tilde{a} = [0.8072 \ 0.0307 \ 0.7606]^\top$. The number of simulation steps is 300 and the attacks are injected into the system as step signals at $k = 100$. The detection threshold is set to $\tau = 16.7496$ given an acceptable false alarm rate $\xi = 0.005$. Fig. 2 illustrates the Mahalanobis distance of residuals $\mathcal{I}(k)$ generated by the Kalman filter under both the optimal attack \bar{a}_{kal}^* and the random attack \tilde{a} , while Fig. 3 shows the corresponding impacts of the two attacks on the state estimation error.

As shown in Fig. 2, under the optimal attack \bar{a}_{kal}^* , the Mahalanobis distance of the residual exceeds the threshold after attack onset, but quickly returns and remains below the threshold. This indicates that \bar{a}_{kal}^* exhibits strong stealthiness and has a low probability of being detected by the Kalman filter. In contrast, the residual induced by the random attack \tilde{a} stays above the threshold after the attack occurs, making it easier to be detected. Fig. 3 further shows that the optimal and random attacks yield comparable magnitudes of state estimation error. This demonstrates that the optimal attack can achieve a similar disruptive effect on the estimation performance of the Kalman filter while maintaining stealthiness.

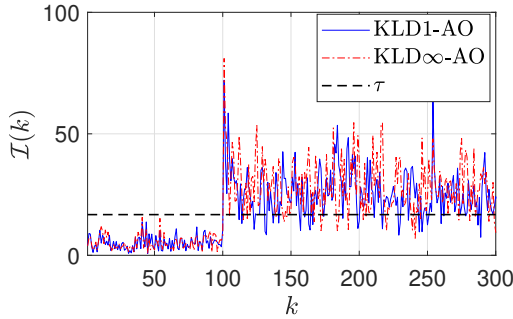


FIGURE 4. Mahalanobis distance using KLD1 and KLD ∞ detectors under respective optimal attacks.

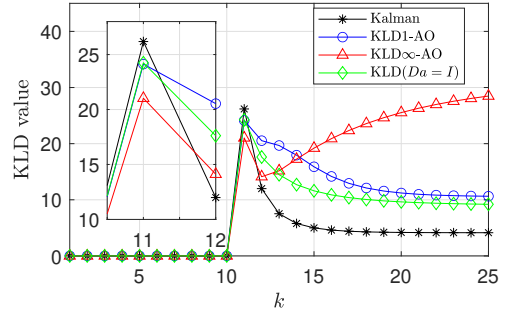


FIGURE 5. KLD values of KLD0, KLD1, and KLD ∞ detectors under \bar{a}_{kal}^* .

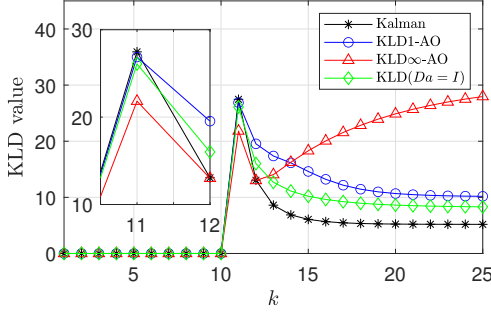


FIGURE 6. KLD values of KLD0, KLD1, and KLD ∞ detectors under \bar{a}_{kld1}^* .

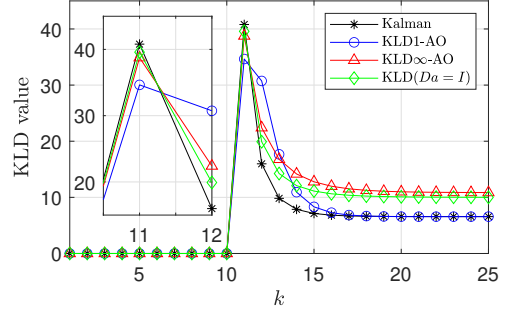


FIGURE 7. KLD values of KLD0, KLD1, and KLD ∞ detectors under $\bar{a}_{kld\infty}^*$.

Step attack scenario. In what follows, we evaluate the performance of the proposed detectors under their corresponding worst-case BIAs. To this end, we first compute the KLD-based observers for $k = 1$ and $k \rightarrow \infty$ using the LMI methods in Theorems 3.6 and 3.9, respectively. Then, following the bi-convex observer design methods in Theorem 3.5 and 3.8 and setting the derived LMI-based detector gains as initial points, we further optimize the observer gains using both the AO and ADMM algorithms. During the optimization, the maximum number of iterations is set to $N_{ite} = 50$, and the stopping tolerance is $\epsilon = 1 \times 10^{-5}$. For the ADMM algorithm, the initial values for the Lagrange multiplier and the step size are chosen as $\Lambda = 0$ and $\eta = 10000$, respectively. The better results between AO and ADMM are selected as the final observer gain, denoted by L_{kld1}^* and $L_{KLD\infty}^*$, respectively. The optimal attacks for KLD1 and KLD ∞ detectors denoted by \bar{a}_{kld1}^* and $\bar{a}_{kld\infty}^*$ are derived as $\bar{a}_{kld1}^* = [0.9167 \ 0.2650 \ 0.2094]^\top$ and $\bar{a}_{kld\infty}^* = [-0.0924 \ 0.9781 \ 0.8206]^\top$, respectively. To illustrate the advantages of explicitly considering attacks on subsets of sensors, we also consider the case where $D_a = I$ and design the detection observer to enhance the attack detectability in the steady-state.

Fig. 4 shows the Mahalanobis distances of residuals generated by KLD1 and KLD ∞ detectors under their respective worst-case BIAs. As illustrated, the Mahalanobis distances for both detectors

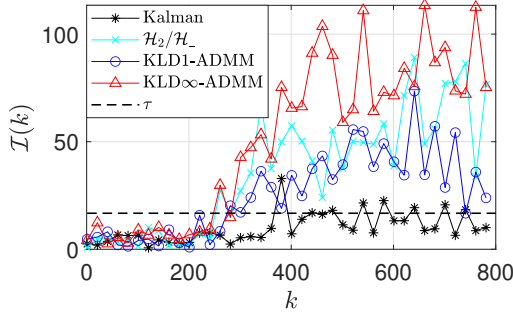


FIGURE 8. Mahalanobis distance by different detectors under the stealthy attacks.

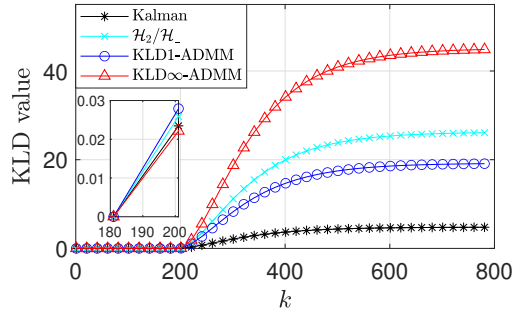


FIGURE 9. KLD values by different detectors under the stealthy attacks.

immediately exceed the threshold upon the attack onset and remain above it thereafter. This demonstrates that the proposed detectors are able to detect the worst-case attacks, while the traditional Kalman filter fails to do so.

Figs. 5-7 depict the KLD values by the proposed KLD-based detectors under the three optimal attacks: \bar{a}_{kal}^* , \bar{a}_{kld1}^* and $\bar{a}_{kld\infty}^*$. A consistent pattern can be observed across all figures. Specifically, as the optimal solution for the case $k = 0$, the Kalman filter achieves the largest KLD value at attack onset. In contrast, the KLD1 detector corresponding to the optimal solution for $k = 1$ attains the largest KLD value at the next instant after the attack, demonstrating the best detection capability during the transient phase. Finally, the KLD ∞ detector yields the largest KLD value as the system approaches steady state. However, when considering $D_a = I$, the resulting KLD ∞ detector achieves smaller KLD values than the KLD1 detector. This highlights the benefit of explicitly accounting for partially compromised sensors in the detector design.

Stealthy attack scenario. In the practical situation, attacks are often slowly injected into sensors to remain stealthy. For example, the attack signal can be implemented as:

$$a(k+1) = (1 - \beta)a(k) + \beta\bar{a}_{kld\infty}^*,$$

where $\beta \in [0, 1]$ determines the injection rate, and we set $\beta = 0.01$ here. Assume that sensors 1, 2, 3, and 5 in the thermal system are compromised. The attack impact matrix W is kept the same as the previous simulation example.

Based on the above setup, we design the KLD1 and KLD ∞ detectors using the methods in Theorems 3.5 and 3.8, respectively. The design procedures and related parameters are identical to those used in the step attack simulation. For comparison, we also include the $\mathcal{H}_2/\mathcal{H}_-$ filter, which is introduced in Subsection 5.2. For fair comparison, we set the upper bound δ as the trace of the covariance matrix of the residual induced by KLD ∞ detector, i.e., $\delta = \text{trace}(\Sigma_{r_\omega}(L_{KLD\infty}^*))$. The simulation results are presented in Figs. 8-10, where the total simulation steps are 800 steps, and the attack occurs at $k = 200$. A data point is plotted every 20 steps.

Fig. 8 presents the Mahalanobis distance generated by different detectors under the stealthy attack. As shown in the figure, the Mahalanobis distance produced by the traditional Kalman filter oscillates around the threshold after the attack occurs, making it unable to detect the attack timely

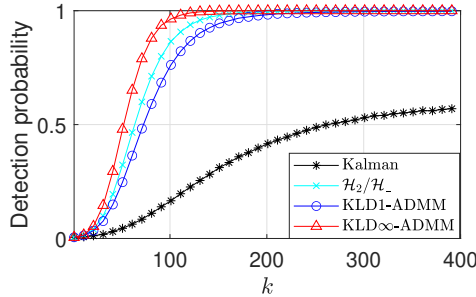


FIGURE 10. Detection probability at each step after the attack occurs.

and reliably. The $\mathcal{H}_2/\mathcal{H}_-$ filter and KLD1 detector show comparable performance. In contrast, the Mahalanobis distance generated by the KLD ∞ detector is larger than all other methods, demonstrating its detection capability in the steady state.

Fig. 9 shows the KLD values generated by these detectors over time, which provides a clearer characterization of detection performance than the Mahalanobis distance. Among all methods, the KLD ∞ detector exhibits the fastest KLD growth rate and the largest steady-state KLD value, indicating the best detection performance. The KLD1 detector achieves the highest KLD value during the transient phase, as depicted in the zoomed-in view, but its steady-state KLD value is lower than that of the $\mathcal{H}_2/\mathcal{H}_-$ filter. These observations are consistent with Fig. 10, which depicts the detection probability over time via Monte Carlo simulations. Specifically, the detection probabilities of the KLD1, KLD ∞ , and $\mathcal{H}_2/\mathcal{H}_-$ filter detectors rapidly approach 1 within a short period, demonstrating their fast detection speed. However, the detection probability of the Kalman filter increases slowly and never reaches a detection probability of one.

6. CONCLUSIONS

This paper proposed design methods for detection observers against BIAs targeting subsets of sensors in stochastic linear systems. By enhancing the detectability of the worst-case BIAs characterized by KLD, we formulate the observer design as a max-min optimization problem, which accounts for the trade-off between attack detectability and its impact. We show that the Kalman filter maximizes the detectability of worst-case BIAs at the attack onset. For the one-step and steady-state scenarios, the resulting design problems are inherently non-convex. We further derived bi-convex formulations and provided LMI relaxations that enable tractable observer synthesis. These results offer a systematic and theoretically grounded approach for stealth-aware detector design in stochastic linear systems. Future work will focus on extending the proposed framework to incorporate active detection mechanisms to address broader classes of adversarial attacks.

APPENDIX A. TECHNICAL PROOFS

We first provide some useful matrix relations and inequalities that are instrumental in later proofs.

Lemma A.1 (Matrix relations). *Let S be a positive definite matrix, X and Y be matrices of appropriate dimensions. The following matrix relations hold:*

- (1) **Young's relation:** $X^\top S^{-1}X \succeq X^\top Y + Y^\top X - Y^\top SY$ as $(X - SY)^\top S^{-1}(X - SY) \succeq 0$.
- (2) **Generalized Young's relation:** $X^\top S^{-1}Y + Y^\top S^{-1}X \preceq \frac{1}{\gamma}X^\top S^{-1}X + \gamma Y^\top S^{-1}Y$ for $\gamma \in \mathbb{R}_+$, because $(\frac{1}{\sqrt{\gamma}}X^\top - \sqrt{\gamma}Y^\top)S^{-1}(\frac{1}{\sqrt{\gamma}}X - \sqrt{\gamma}Y) \succeq 0$.
- (3) **Binomial inverse theorem:** $(S + XY)^{-1} = S^{-1} - S^{-1}X(I + YS^{-1}X)^{-1}YS^{-1}$ provided $I + YS^{-1}X$ is not singular.

Proof of Theorem 3.6. Applying Schur complement to (18b) leads to

$$\begin{aligned} & \begin{bmatrix} Y^\top D_a + D_a^\top Y & D_a^\top R_W^\top \\ R_W D_a & 2\mu I \end{bmatrix} - \begin{bmatrix} \Gamma_1 & 0 \\ 0 & \mu I \end{bmatrix} \begin{bmatrix} \Gamma_2 & 0 \\ 0 & \mu I \end{bmatrix}^{-1} \begin{bmatrix} \Gamma_1^\top & 0 \\ 0 & \mu I \end{bmatrix} \\ &= \begin{bmatrix} Y^\top D_a + D_a^\top Y & D_a^\top R_W^\top \\ R_W D_a & 2\mu I \end{bmatrix} - \begin{bmatrix} \Gamma_1 \Gamma_2^{-1} \Gamma_1^\top & 0 \\ 0 & \mu I \end{bmatrix} \succeq 0, \end{aligned} \quad (24)$$

where $\Gamma_1 \Gamma_2^{-1} \Gamma_1^\top = (2 + 1/\gamma)Y^\top CP^{-1}C^\top Y + \gamma D_a^\top G^\top P^{-1}GD_a + 2Y^\top D_\omega D_\omega^\top Y$. Based on the generalized Young's relation in Lemma A.1, it holds that

$$\frac{1}{\gamma}Y^\top CP^{-1}C^\top Y + \gamma D_a^\top G^\top P^{-1}GD_a \succeq Y^\top CP^{-1}GD_a + D_a^\top G^\top P^{-1}C^\top Y.$$

Therefore, $\Gamma_1 \Gamma_2^{-1} \Gamma_1^\top \succeq 2Y^\top (CP^{-1}C^\top + D_\omega D_\omega^\top)Y + Y^\top CP^{-1}GD_a + D_a^\top G^\top P^{-1}C^\top Y$. Together with the inequality (24), we have

$$\begin{aligned} & \begin{bmatrix} Y^\top D_a + D_a^\top Y & D_a^\top R_W^\top \\ R_W D_a & 2\mu I \end{bmatrix} - \begin{bmatrix} Y^\top CP^{-1}GD_a + D_a^\top G^\top P^{-1}C^\top Y & 0 \\ + 2Y^\top (CP^{-1}C^\top + D_\omega D_\omega^\top)Y & 0 \end{bmatrix} \\ &= \begin{bmatrix} \varphi(Y, L) - 2Y^\top (CP^{-1}C + D_\omega D_\omega^\top)Y & D_a^\top R_W^\top \\ R_W D_a & \mu I \end{bmatrix} \succeq 0, \end{aligned}$$

where $L = P^{-1}G$ and $\varphi(Y, L) := Y^\top (I - CL)D_a + D_a^\top (I - CL)^\top Y$. Again, utilizing the Schur complement yields

$$\varphi(Y, L) - 2Y^\top (CP^{-1}C + D_\omega D_\omega^\top)Y - \lambda D_a^\top WD_a \succeq 0,$$

where $\mu = 1/\lambda$ and $W = R_W^\top R_W$. Moreover, according to Lemma 3.2, inequalities (12) ensure that $\rho(A - LC) < 1$ and $\Sigma_{r_\omega}^{-1}(L) \succ (CP^{-1}C^\top + D_\omega D_\omega^\top)^{-1} \succ \tilde{Z}$. Therefore, it holds that $\varphi(Y, L) - 2Y^\top \Sigma_{r_\omega}(L)Y - \lambda D_a^\top WD_a \succeq 0$. Recall the inequality (16), we obtain

$$\frac{1}{2}D_a^\top (I - CL)^\top \Sigma_{r_\omega}^{-1}(L)(I - CL)D_a - \lambda D_a^\top WD_a \succeq 0,$$

This proves the sufficiency of the conditions (18) for (14). Finally, by maximizing $1/\mu$ (equivalent to minimizing μ) with the obtained sufficient conditions, we obtain the approximated optimization problem in Theorem 3.6, which completes the proof. \square

Proof of Lemma 3.7. Setting $S = I - A$, $X = L$, and $Y = C$ in the Binomial inverse theorem in Lemma A.1 yields

$$\begin{aligned} & C(I - A + LC)^{-1}L \\ &= C(I - A)^{-1}L - C(I - A)^{-1}L(I + C(I - A)^{-1}L)^{-1}C(I - A)^{-1}L \\ &= ML - ML(I + ML)^{-1}ML. \end{aligned}$$

Note that $ML - ML(I + ML)^{-1}ML$ is the expansion of $((ML)^{-1} + I)^{-1}$ based on the Binomial inverse theorem by setting $S = (ML)^{-1}$, $X = Y = I$. The inverse term $((ML)^{-1} + I)^{-1}$ can be further written as

$$((ML)^{-1} + I)^{-1} = ((ML)^{-1} + I)^{-1} (ML)^{-1}ML = (I + ML)^{-1}ML.$$

Therefore, we have $C(I - A + LC)^{-1}L = (I + ML)^{-1}ML$. Substituting this equality into $\Phi(\infty, L)$ leads to

$$\begin{aligned} \Phi(\infty, L) &= I - (I + ML)^{-1}ML \\ &= (I + ML)^{-1}(I + ML) - (I + ML)^{-1}ML = (I + ML)^{-1}. \end{aligned}$$

This completes the proof. \square

Proof of Theorem 3.9. Applying the Schur complement to (23) leads to

$$\Theta_1 - \begin{bmatrix} \Theta_2 & \Theta_3 \\ 0 & \frac{1}{\gamma}P^{-1} \end{bmatrix} \begin{bmatrix} \gamma P^{-1} & 0 \\ 0 & \frac{1}{\gamma}P^{-1} \end{bmatrix} \begin{bmatrix} \Theta_2^\top \\ \Theta_3^\top \end{bmatrix} = \Theta_1 - \gamma\Theta_2 P^{-1} \Theta_2^\top - \frac{1}{\gamma}\Theta_3 P^{-1} \Theta_3^\top \succeq 0.$$

According to the generalized Young's relation in Lemma A.1, it holds that

$$-\Theta_2 P^{-1} \Theta_3^\top - \Theta_3 P^{-1} \Theta_2^\top \succeq -\gamma\Theta_2 P^{-1} \Theta_2^\top - \frac{1}{\gamma}\Theta_3 P^{-1} \Theta_3^\top.$$

As a result, we have

$$\begin{aligned} &\Theta_1 - \Theta_2 P^{-1} \Theta_3^\top - \Theta_3 P^{-1} \Theta_2^\top \\ &= \begin{bmatrix} D_a^\top Y + Y^\top D_a - \lambda D_a^\top W D_a & Y^\top(I + ML) \\ * & \frac{1}{2}\tilde{Z} \end{bmatrix} \succeq 0, \end{aligned}$$

where $L = P^{-1}G$. Again, utilizing the Schur complement, the above inequality can be further written as

$$D_a^\top Y + Y^\top D_a - 2Y^\top(I + ML)\tilde{Z}^{-1}(I + ML)^\top Y - \lambda D_a^\top W D_a \succeq 0.$$

Based on Lemma 3.2, conditions (18a) ensure that $\rho(A - LC) < 1$ and $\Sigma_{r_\omega}^{-1}(L) \succ \tilde{Z}$. As a result, the following inequalities hold

$$\begin{aligned} &\frac{1}{2}D_a^\top(I + ML)^{-\top}\Sigma_{r_\omega}(L)^{-1}(I + ML)^{-1}D_a - \lambda D_a^\top W D_a \\ &\succeq D_a^\top Y + Y^\top D_a - 2Y^\top(I + ML)\Sigma_{r_\omega}(L)(I + ML)^\top Y - \lambda D_a^\top W D_a \succeq 0, \end{aligned}$$

where the first inequality has been proved in (22). The satisfaction of constraints in (19) under conditions in (23) is thus demonstrated. This completes the proof. \square

REFERENCES

- [1] S. H. Ahmed, G. Kim, D. Kim, Cyber physical system: Architecture, applications and research challenges, 2013 IFIP Wireless Days (WD) (2013) 1–5.
- [2] C. Peng, H. Sun, M. Yang, Y.-L. Wang, A survey on security communication and control for smart grids under malicious cyber attacks, *IEEE Transactions on Systems, Man, and Cybernetics: Systems* 49 (8) (2019) 1554–1569.
- [3] Y. Jiang, S. Wu, R. Ma, M. Liu, H. Luo, O. Kaynak, Monitoring and defense of industrial cyber-physical systems under typical attacks: From a systems and control perspective, *IEEE Transactions on Industrial Cyber-Physical Systems* 1 (2023) 192–207.

- [4] A. Cardenas, S. Amin, B. Sinopoli, A. Giani, A. Perrig, S. Sastry, et al., Challenges for securing cyber physical systems, in: Workshop on future directions in cyber-physical systems security, Vol. 5, 2009, p. 7.
- [5] Z. Guo, D. Shi, K. H. Johansson, L. Shi, Worst-case stealthy innovation-based linear attack on remote state estimation, *Automatica* 89 (2018) 117–124.
- [6] Q. Zhang, K. Liu, Y. Xia, A. Ma, Optimal stealthy deception attack against cyber-physical systems, *IEEE Transactions on Cybernetics* 50 (9) (2019) 3963–3972.
- [7] A. Teixeira, I. Shames, H. Sandberg, K. H. Johansson, A secure control framework for resource-limited adversaries, *Automatica* 51 (2015) 135–148.
- [8] Y. Mo, B. Sinopoli, Secure control against replay attacks, in: 2009 47th annual Allerton conference on communication, control, and computing (Allerton), IEEE, 2009, pp. 911–918.
- [9] H. Zhang, P. Cheng, L. Shi, J. Chen, Optimal dos attack scheduling in wireless networked control system, *IEEE Transactions on Control Systems Technology* 24 (3) (2015) 843–852.
- [10] C. Fang, Y. Qi, P. Cheng, W. X. Zheng, Optimal periodic watermarking schedule for replay attack detection in cyber-physical systems, *Automatica* 112 (2020) 108698.
- [11] A.-Y. Lu, G.-H. Yang, Attack detection from the perspectives of control center and controlled systems, *IEEE Transactions on Automatic Control* 69 (12) (2024) 8662–8673.
- [12] H. Liu, Y. Li, Q.-L. Han, T. Raïssi, T. Chai, Secure estimation, attack isolation, and reconstruction based on zonotopic unknown input observer, *IEEE Transactions on Automatic Control* 68 (12) (2023) 7312–7325.
- [13] S. Hu, X. Chen, J. Li, X. Xie, Observer-based resilient controller design for networked stochastic systems under coordinated dos and fdi attacks, *IEEE Transactions on Control of Network Systems* 11 (2) (2023) 890–901.
- [14] X. Wang, X. Luo, X. Pan, X. Guan, Detection and location of bias load injection attack in smart grid via robust adaptive observer, *IEEE Systems Journal* 14 (3) (2020) 4454–4465.
- [15] M. Liu, X. Zhang, R. Zhang, Z. Zhou, Z. Zhang, R. Deng, Detection-triggered recursive impact mitigation against secondary false data injection attacks in cyber-physical microgrids, *IEEE Transactions on Smart Grid* (2024).
- [16] T. Tanaka, K. Sawada, Y. Watanabe, M. Iwamoto, Covert vehicle misguidance and its detection: A hypothesis testing game over continuous-time dynamics, *IEEE Control Systems Letters* (2024).
- [17] H. Liu, Y. Zhang, Y. Li, B. Niu, Proactive attack detection scheme based on watermarking and moving target defense, *Automatica* 155 (2023) 111163.
- [18] A. Naha, A. M. Teixeira, A. Ahlén, S. Dey, Quickest detection of deception attacks on cyber-physical systems with a parsimonious watermarking policy, *Automatica* 155 (2023) 111147.
- [19] K. Manandhar, X. Cao, F. Hu, Y. Liu, Detection of faults and attacks including false data injection attack in smart grid using kalman filter, *IEEE transactions on control of network systems* 1 (4) (2014) 370–379.
- [20] C. Murguia, J. Ruths, On model-based detectors for linear time-invariant stochastic systems under sensor attacks, *IET Control Theory & Applications* 13 (8) (2019) 1051–1061.
- [21] N. Ahmed, A. Ameli, H. Naser, Detection, identification, and mitigation of false data injection attacks in vehicle platooning, *IEEE Transactions on Vehicular Technology* (2024).
- [22] X. Huang, J. Li, Q. Su, An observer with cooperative interaction structure for biasing attack detection and secure control, *IEEE Transactions on Systems, Man, and Cybernetics: Systems* 53 (4) (2022) 2543–2553.
- [23] H. Liu, S. Wang, B. Niu, Y. Li, A novel attack detection for linear systems with unknown-but-bounded noises, *IEEE Transactions on Systems, Man, and Cybernetics: Systems* 52 (7) (2021) 4223–4232.
- [24] J. Li, Z. Wang, Y. Shen, L. Xie, Attack detection for cyber-physical systems: A zonotopic approach, *IEEE Transactions on Automatic Control* 68 (11) (2023) 6828–6835.
- [25] F. Pasqualetti, F. Dörfler, F. Bullo, Attack detection and identification in cyber-physical systems, *IEEE Transactions on Automatic Control* 58 (11) (2013) 2715–2729.
- [26] S. Cui, Z. Han, S. Kar, T. T. Kim, H. V. Poor, A. Tahir, Coordinated data-injection attack and detection in the smart grid: A detailed look at enriching detection solutions, *IEEE Signal Processing Magazine* 29 (5) (2012) 106–115.
- [27] Y. Mo, R. Chabukswar, B. Sinopoli, Detecting integrity attacks on scada systems, *IEEE Transactions on Control Systems Technology* 22 (4) (2013) 1396–1407.

- [28] C.-Z. Bai, F. Pasqualetti, V. Gupta, Data-injection attacks in stochastic control systems: Detectability and performance tradeoffs, *Automatica* 82 (2017) 251–260.
- [29] G. Chaojun, P. Jirutitijaroen, M. Motani, Detecting false data injection attacks in ac state estimation, *IEEE Transactions on Smart Grid* 6 (5) (2015) 2476–2483.
- [30] R. Deng, G. Xiao, R. Lu, Defending against false data injection attacks on power system state estimation, *IEEE Transactions on Industrial Informatics* 13 (1) (2015) 198–207.
- [31] A. Teixeira, I. Shames, H. Sandberg, K. H. Johansson, Revealing stealthy attacks in control systems, in: 2012 50th Annual Allerton Conference on Communication, Control, and Computing (Allerton), IEEE, 2012, pp. 1806–1813.
- [32] F. E. Tosun, A. M. Teixeira, J. Dong, A. Ahlén, S. Dey, Kullback-leibler divergence-based filter design against bias injection attacks, *European Journal of Control* (2025) 101427.
- [33] Y. Feng, D. Lan, C. Shang, False data-injection attack detection in cyber-physical systems: A wasserstein distributionally robust reachability optimization approach, *arXiv preprint arXiv:2508.12402* (2025).
- [34] J. Milošević, T. Tanaka, H. Sandberg, K. H. Johansson, Analysis and mitigation of bias injection attacks against a kalman filter, *IFAC-PapersOnLine* 50 (1) (2017) 8393–8398.
- [35] Y. Chen, S. Kar, J. M. Moura, Cyber-physical attacks with control objectives, *IEEE Transactions on Automatic Control* 63 (5) (2017) 1418–1425.
- [36] S. Kullback, *Information theory and statistics*, Courier Corporation, 1997.
- [37] B. Ghojogh, F. Karray, M. Crowley, Eigenvalue and generalized eigenvalue problems: Tutorial, *arXiv preprint arXiv:1903.11240* (2019).
- [38] S. P. Boyd, L. Vandenberghe, *Convex optimization*, Cambridge university press, 2004.
- [39] J. P. Hespanha, *Linear systems theory*, Princeton university press, 2018.
- [40] N. Yang, Z. Wang, T. Yang, Y. Li, L. Shi, Lasso-based detection and identification of actuator integrity attacks in remote control systems, *IEEE Transactions on Control Systems Technology* 32 (2) (2023) 696–704.
- [41] J. Dong, K. Pan, S. Pequito, P. M. Esfahani, Robust multivariate detection and estimation with fault frequency content information, *Automatica* 173 (2025) 112049.